

CONSTRAINTS ON SHALLOW ⁵⁶Ni FROM THE EARLY LIGHTCURVES OF TYPE IA SUPERNOVAE

ANTHONY L. PIRO¹ AND EHUD NAKAR²

Submitted for publication in The Astrophysical Journal

ABSTRACT

Ongoing transient surveys are presenting an unprecedented account of the rising lightcurves of Type Ia supernovae (SNe Ia). This early emission probes the shallowest layers of the exploding white dwarf, which can provide constraints on the progenitor star and the properties of the explosive burning. We use semi-analytic models of radioactively-powered rising lightcurves to analyze these observations. As we have summarized in previous work, the main limiting factor in determining the surface distribution of ⁵⁶Ni is the lack of an unambiguously identified time of explosion, as would be provided by detection of shock breakout or shock-heated cooling. Without this the SN may in principle exhibit a “dark phase” for a few hours to days, where the only emission is from shock-heated cooling that is too dim to be detected. Nevertheless, by considering the time-dependent velocity evolution, the explosion time can be better constrained, albeit with considerable uncertainty. This technique is used to infer the surface ⁵⁶Ni distribution of three recent SNe Ia that were caught especially early in their rise. Although we cannot constrain the explosion times to better than ≈ 1 day, in all three we find fairly similar ⁵⁶Ni distributions. Observations of SN 2011fe and SN 2012cg probe shallower depths than in SN 2009ig, and in these two cases ⁵⁶Ni is present merely $\approx 10^{-2}M_{\odot}$ from the WD’s surface. We also use our conclusions about the explosion times to reassess radius constraints for the progenitor of SN 2011fe, as well as discuss the roughly t^2 power law that is inferred for many observed rising lightcurves.

Subject headings: hydrodynamics — shock waves — supernovae: general — white dwarfs

1. INTRODUCTION

Type Ia supernovae (SNe Ia) play a central role in modern astrophysics. They are used as distance indicators to probe the expansion of the Universe (Riess et al. 1998; Perlmutter et al. 1999), they produce most of the iron-group elements in the cosmos (Iwamoto et al. 1999), and they provide an astrophysical context for studying explosions (Hillebrandt & Niemeyer 2000). But their importance has brought attention to the theoretical uncertainties that frustratingly remain. It is generally accepted that they result from unstable thermonuclear ignition of degenerate matter (Hoyle & Fowler 1960) in a C/O white dwarf (WD), but the progenitor systems have not been identified. Candidates include stable accretion from a non-degenerate binary companion (Whelan & Iben 1973), the merging of two C/O WDs (Iben & Tutukov 1984; Webbink 1984), or accretion and detonation of a helium shell on a C/O WD that leads to core detonation (Woosley & Weaver 1994a; Livne & Arnett 1995). In addition, it is not known whether the incineration proceeds as a sub-sonic deflagration (Nomoto et al. 1976, 1984) or deflagration-detonation transition (DDT; Khokhlov 1991; Woosley & Weaver 1994b). Each scenario has implications for the velocity profile, density structure, and distribution of ashes within the exploding WD.

A powerful method for constraining between these models is the study of the early-time behavior of SNe Ia, since this is when the shallowest layers of the WD are probed by the observed emission. Analysis of spectra provides one way of learning about the surface abundances of these explosions (e.g., Hachinger et al. 2012). The photometry is also sensitive to the depth and distribution of radioactive heating (Piro 2012; Piro & Nakar 2012). With early observations of SNe Ia

becoming more common, the time is ripe to explore what can be learned from these measurements.

In the following work we use semi-analytic models to study where and how much ⁵⁶Ni is present in the outer ejecta of SNe Ia. As discussed in our previous investigation of radioactively-powered lightcurves (Piro & Nakar 2012), it is difficult to directly measure the ⁵⁶Ni distribution without a detection of the explosion time, as would be provided by shock breakout or shock-heated cooling (Piro et al. 2010; Nakar & Sari 2010; Nakar & Sari 2012; Rabinak et al. 2012). Unfortunately, in the case of SNe Ia, such emission has never been detected because of the small WD radius. If merely photometric lightcurves of the rise are available, there is a degeneracy between emission being from ⁵⁶Ni near the surface with a recent explosion versus ⁵⁶Ni deeper in the star but with an explosion further in the past. In the latter case, a SN Ia exhibits a “dark phase” for a few hours to days until the thermal diffusion wave reaches the shallowest ⁵⁶Ni deposits. Even with these uncertainties, constraints can still be provided by comparing a wider range of properties, such as the velocity evolution. This information is available for a few well-studied SNe Ia, and we use it in order to estimate the time of explosion and surface ⁵⁶Ni distribution for each of them.

In §2 we summarize the semi-analytic framework used to model the rising lightcurves. In §3 we analyze observations of three recent SNe Ia and summarize our constraints on their shallow ⁵⁶Ni distributions. In §4 we consider the t^2 rise that is often observed in early lightcurves and discuss whether t^2 (or any power-law) should be expected. We conclude in §5 with a summary of our results and a discussion of future work.

2. RADIOACTIVELY-POWERED RISING LIGHTCURVES

In the following we present the model used for this study, which borrows from and builds upon our recent work on

¹ Theoretical Astrophysics, California Institute of Technology, 1200 E California Blvd., M/C 350-17, Pasadena, CA 91125; piro@caltech.edu

² Raymond and Beverly Sackler School of Physics and Astronomy, Tel Aviv University, Tel Aviv 69978, Israel

radioactively-powered rising lightcurves. In Piro (2012) we focused on direct ^{56}Ni heating at the depth of the diffusion wave. In Piro & Nakar (2012) we added the ‘‘diffusive tail,’’ which provides heating at depths shallower than the intrinsic ^{56}Ni distribution. Here we include these effects in greater detail by integrating over their contributions throughout the WD, as discussed in Appendix B of Piro & Nakar (2012).

As the ejecta from the SN expands, a thermal diffusion wave travels back through the material. At any time t , the diffusion wave has a depth of roughly

$$\Delta M_{\text{diff}} \approx 2 \times 10^{-2} \frac{E_{51}^{0.44}}{\kappa_{0.1}^{0.88} M_{1.4}^{0.32}} \left(\frac{t}{1 \text{ day}} \right)^{1.76} M_{\odot}, \quad (1)$$

where $E = 10^{51} E_{51} \text{ erg}$ is the explosion energy, and $M = 1.4 M_{1.4} M_{\odot}$ is the ejecta mass, and $\kappa = 0.1 \kappa_{0.1} \text{ cm}^2 \text{ g}^{-1}$ is the opacity. We approximate the opacity as constant, which is roughly correct for the temperatures of interest (Pinto & Eastman 2000). The scalings and prefactors in equation (1) use Appendix C of Piro & Nakar (2012) with values appropriate for Chandrasekhar mass WDs.

At early times the ejecta is optically thick to gamma-rays emitted from radioactive decay, and they efficiently heat the SN. Heating in material shallower than ΔM_{diff} directly goes into the observed luminosity. Heating in material deeper than ΔM_{diff} only contributes to the observed lightcurve if some fraction of the photons from these larger depths are able to diffuse up to ΔM_{diff} . In Piro & Nakar (2012), we demonstrated that if some depth in the ejecta would be reached by the diffusion wave at time t' , then at times $t < t'$ the fraction of photons that would escape from this depth are

$$\text{Escaping fraction} \approx \text{erfc}(t'/\sqrt{2}t) \quad (2)$$

where erfc is the complementary error function. This provides the so-called diffusive tail.

Motivated by this picture, we split the total observed luminosity into two parts

$$L(t) = L_{56}(t) + L_{\text{tail}}(t), \quad (3)$$

where L_{56} is the direct heating by ^{56}Ni down to ΔM_{diff} , and L_{tail} is the diffusive tail from material deeper than ΔM_{diff} . Each is an integral over different regions of the ejecta. For the direct heating component

$$L_{56}(t) = \int_0^t X_{56}(t') \frac{\partial \Delta M_{\text{diff}}}{\partial t'} \epsilon(t) dt', \quad (4)$$

where $X_{56}(t)$ is the mass fraction of ^{56}Ni at the depth of the diffusion wave at time t , and the specific heating rate is

$$\epsilon(t) = \epsilon_{\text{Ni}} e^{-t/t_{\text{Ni}}} + \epsilon_{\text{Co}} (e^{-t/t_{\text{Co}}} - e^{-t/t_{\text{Ni}}}), \quad (5)$$

where $\epsilon_{\text{Ni}} = 3.9 \times 10^{10} \text{ erg g}^{-1} \text{ s}^{-1}$, $t_{\text{Ni}} = 8.76 \text{ days}$, $\epsilon_{\text{Co}} = 7.0 \times 10^9 \text{ erg g}^{-1} \text{ s}^{-1}$, and $t_{\text{Co}} = 111.5 \text{ days}$. The total diffusive tail component is the integral over all the diffusive tails from heating deeper than ΔM_{diff} ,

$$L_{\text{tail}}(t) = \int_t^{t_{\text{diff}}} X_{56}(t') \frac{\partial \Delta M_{\text{diff}}}{\partial t'} \epsilon(t) \frac{\text{erfc}(t'/\sqrt{2}t)}{\text{erfc}(1/\sqrt{2})} dt'. \quad (6)$$

We take the upper integration limit to be the diffusion time through the entire ejecta t_{diff}^3 , which roughly corresponds to

³ Note that in this work we are using a different definition of t_{diff} than that in Piro & Nakar (2012).

the time of lightcurve peak.

Since $\Delta M_{\text{diff}} \propto t^{1.76}$, equations (4) and (6) are rewritten as

$$L_{56}(t) = 1.76 L_0(t) \int_0^t \frac{X_{56}(t')}{X_{56}(t)} \left(\frac{t'}{t} \right)^{1.76} \frac{dt'}{t'}, \quad (7)$$

and

$$L_{\text{tail}}(t) = 1.76 L_0(t) \int_t^{t_{\text{diff}}} \frac{X_{56}(t')}{X_{56}(t)} \left(\frac{t'}{t} \right)^{1.76} \frac{\text{erfc}(t'/\sqrt{2}t)}{\text{erfc}(1/\sqrt{2})} \frac{dt'}{t'}, \quad (8)$$

where $L_0(t) \equiv X_{56}(t) \Delta M_{\text{diff}}(t) \epsilon(t)$ is roughly the local heating rate from ^{56}Ni . The luminosity has no contribution from the diffusive tail once the diffusion wave has travelled through the ejecta, thus we define $L_{\text{diff}} \equiv L_{56}(t = t_{\text{diff}})$.

When actually performing calculations, it is useful to write these expressions in dimensionless forms. First, let $x \equiv t/t_{\text{diff}}$ and $x' \equiv t'/t_{\text{diff}}$, where x and x' vary from 0 to 1. We define the ratio of the local heating rate to L_{diff} as

$$\begin{aligned} \Lambda(x) &\equiv 1.76 \frac{L_0(x)}{L_{\text{diff}}} \\ &= \frac{\epsilon(x)}{\epsilon(1)} \left[\int_0^1 \frac{X_{56}(x')}{X_{56}(x)} \left(\frac{x'}{x} \right)^{1.76} \frac{dx'}{x'} \right]^{-1}. \end{aligned} \quad (9)$$

The ratio of the observed time-dependent luminosity to L_{diff} is then

$$\begin{aligned} \frac{L(x)}{L_{\text{diff}}} &= \Lambda(x) \int_0^x \frac{X_{56}(x')}{X_{56}(x)} \left(\frac{x'}{x} \right)^{1.76} \frac{dx'}{x'} \\ &+ \Lambda(x) \int_x^1 \frac{X_{56}(x')}{X_{56}(x)} \left(\frac{x'}{x} \right)^{1.76} \frac{\text{erfc}(x'/\sqrt{2}x)}{\text{erfc}(1/\sqrt{2})} \frac{dx'}{x'}. \end{aligned} \quad (10)$$

In this form the right-hand side is dimensionless and only depends on the ^{56}Ni distribution. This allows us to vary $X_{56}(x)$ and calculate a wide range of lightcurves, which can then be rescaled to a particular observation via L_{diff} and t_{diff} . When fitting a ^{56}Ni distribution to a given lightcurve in the next section, we use the parametrization

$$X_{56}(x) = \frac{X'_{56}}{1 + \exp[-\beta(x - x_{1/2})]}, \quad (11)$$

where X'_{56} sets the normalization, β controls the steepness of the rise, and $x_{1/2}$ is the time when $X_{56}/X'_{56} = 1/2$. This allows us to consider a variety of ^{56}Ni distributions with two parameters. The normalization is determined by

$$\begin{aligned} X'_{56} &= \frac{L_{\text{diff}}}{1.76 \Delta M_{\text{diff}}(t_{\text{diff}}) \epsilon(t_{\text{diff}})} \\ &\times \left[\int_0^1 \frac{x'^{0.76} dx'}{1 + \exp[-\beta(x' - x_{1/2})]} \right]^{-1}, \end{aligned} \quad (12)$$

and thus is not a free parameter.

3. COMPARISONS TO SPECIFIC SUPERNOVAE

Recent observations have been especially fruitful in catching SNe Ia at early times. We use this work to analyze three well-studied events: SN 2011fe, SN 2012cg, and SN 2009ig. For each we summarize what can be constrained from their photometric lightcurves and velocity evolution. Although

there are particular issues for each event (which we discuss below), our general strategy is as follows.

1. Since a SN may in principle exhibit a dark phase, we assume that the time of explosion is not known.
2. For a spectral line generated at constant specific opacity, its velocity is a power law with time with $v \propto t^{-0.22}$ (Piro & Nakar 2012). We vary the explosion time and check when the observed absorption features best match this power-law⁴. From this we infer what is the likely explosion time.
3. The photospheric velocity v_{ph} is expected to roughly follow the low-velocity Si II $\lambda 6355$ absorption feature (Tanaka et al. 2008). Using the fits performed in the previous step, we can therefore estimate $v_{\text{ph}}(t)$. The photospheric radius is then given by $r_{\text{ph}} = v_{\text{ph}}t$.
4. Assuming that the SN emits roughly as a blackbody and using the observed B , V , and R lightcurves, we fit the color temperature T_c and bolometric luminosity as a function of time using $L \approx 4\pi r_{\text{ph}}^2 \sigma_{\text{SB}} T_c^4$.
5. Theoretical lightcurves are generated with different $X_{56}(x)$ via equation (10), where $X_{56}(x)$ has the functional form of equation (11). We estimate L_{diff} and t_{diff} as roughly the peak luminosity and time of peak luminosity, respectively. In this way the theoretical lightcurves are rescaled for comparison with the bolometric lightcurve, and we can put constraints on what is the most likely distribution of ^{56}Ni .

3.1. Modeling SN 2011fe

We first focus on SN 2011fe because it is the most constrained by our modeling. SN 2011fe exploded in August 2011 as the closest SNe Ia in the last 25 years (Nugent et al. 2011). The considerable interest in this event and its proximity make it one of the best studied SNe Ia. The time-dependent velocities of absorption features are summarized in Parrent et al. (2012). The B , V , and R rising lightcurves are presented in Vinkó et al. (2012). This particular work was chosen because of the high density of observations during the rise, but we could have just as well considered other data sets (Munari et al. 2012; Richmond & Smith 2012). We use a distance modulus for M101 of 29.05 (Shappee & Stanek 2011), and no reddening is included because it has been inferred to be relatively small (Patat et al. 2011). The various studies have found different time for the peak bolometric luminosity, depending on the fitting method used. For the present work we choose a time of peak of JD 2455815.4, although this choice does not greatly impact our conclusions for the ^{56}Ni distribution at shallow depths. The earliest detection was at JD 2455797.65 (Nugent et al. 2011), and their fitting of a t^2 power law to the rising luminosity, (as is common practice) gives an explosion time of JD 2455797.2 before the peak. Although they quote an error of ± 0.01 days, as we discuss

⁴ The fact that we find that all of the absorption features obey roughly the same power-law dependence is interesting in and of itself and deserves some discussion. It indicates that different features are due to different line opacities within a flow with the same velocity power-law profile and are not separate velocity components in the ejecta. This argues against situations where the high velocity features are generated by a separate event during or prior to the explosion (e.g., Piro 2011).

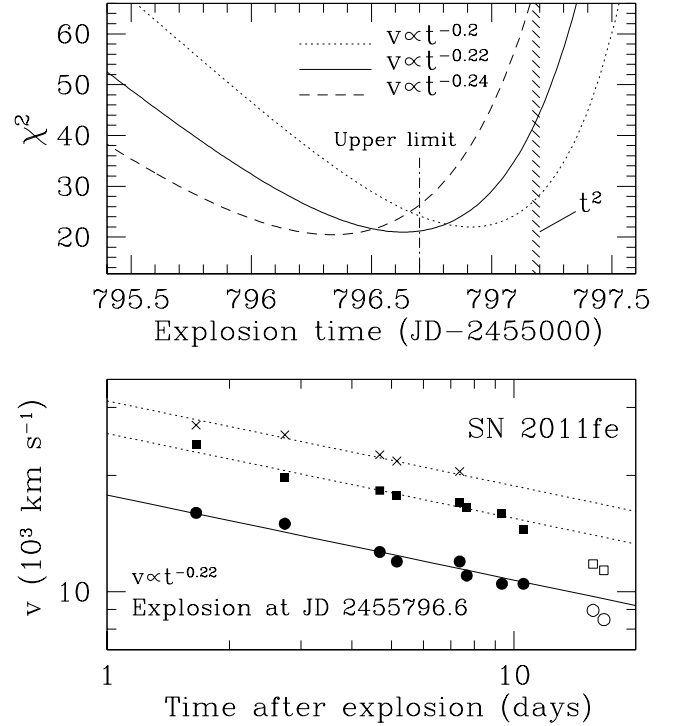


FIG. 1.— The top panel plots the χ^2 found by fitting the velocity evolution as a power law with time for different explosion times and various power-law indices as labeled. We draw vertical dot-dashed line at the time of an upper limit from a non-detection and a shaded region at the explosion time inferred by fitting a t^2 rise (Nugent et al. 2011). In the bottom panel we plot the observed low-velocity Si II $\lambda 6355$ (circles), high-velocity Si II $\lambda 6355$ (squares), and high-velocity Ca II H&K (crosses). Filled and open symbols indicate data that was used or not used for the fit, respectively. The lines show our best fit velocity evolution for $v \propto t^{-0.22}$, and the solid line indicates the v_{ph} we use in subsequent analysis.

later this practice is not well justified and the true uncertainty in the explosion time is considerably larger. Nugent et al. (2011) also observed the location of SN 2011fe roughly at JD 2455796.7, which provides an upper limit in the apparent g -band magnitude of 21.5 (absolute magnitude of -7.55).

In our analysis of the velocity evolution, we use the low-velocity Si II $\lambda 6355$, high-velocity Si II $\lambda 6355$, and high-velocity Ca II H&K absorption features⁵. In the top panel of Figure 1 we plot the χ^2 found by fitting these features with power-law velocity profiles as a function of the explosion time, where χ^2 is defined as

$$\chi^2 = \sum_N \left(\frac{v_N - v(t)}{\Delta v} \right)^2, \quad (13)$$

where N is the number of data points, v_N is a measured velocity, and $\Delta v = 500 \text{ km s}^{-1}$ is a rough estimate of the measurement error (Parrent et al. 2012). The reduced χ^2 around the best fit explosion time is about 1.2 (there are 17 degrees of freedom). In Figure 1 we consider three different velocity power-law indices centered around the model prediction of $v \propto t^{-0.22}$. This shows that the model provides a good description of the data, and that assuming that the power-law index is known, the explosion time is measured to within about ± 0.25

⁵ Other absorption features are measured, but we restrict our study to these three since they are some of the most widely available in SN Ia literature.

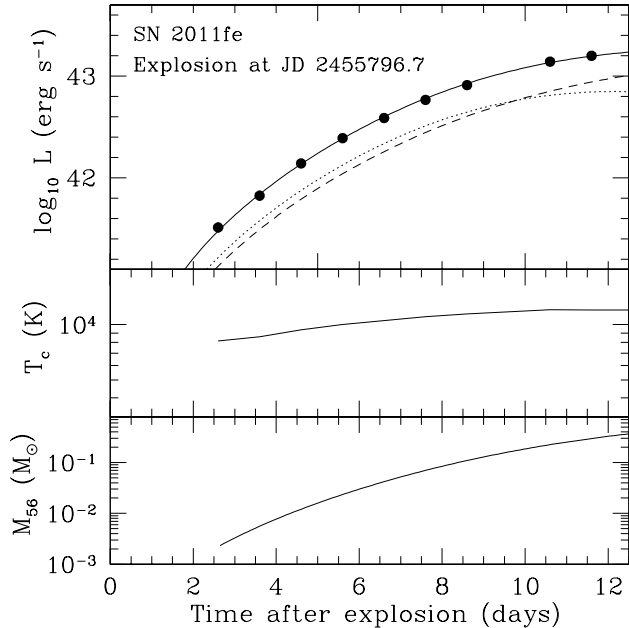


FIG. 2.— A summary of the fits to SN 2011fe. The top panel shows the inferred bolometric luminosity (filled circles) and fit bolometric luminosity (solid curve), which is composed of L_{56} (dashed curve) and L_{tail} (dotted curve). The middle panel shows the color temperature, and the bottom panel shows $M_{56} = L_{56}/\epsilon$.

days. However, assuming slightly different power-laws produces fits with similar quality and results in explosion times that vary by about ≈ 1 day. Since theoretically $v \propto t^{-0.22}$ is the preferred velocity profile we consider JD 2455796.6 to be the most likely explosion time with an uncertainty of roughly ± 0.5 day. This is actually very similar (within 0.1 days) of the non-detection by Nugent et al. (2011). In the bottom panel we present the velocity data along with our best-fit velocity evolutions. Open symbols indicate data that were not used for the fit because they are near peak where the velocity profile is not expected to be a power law.

For any given explosion time we can look for the ^{56}Ni that produces the observed luminosity. The results from fitting the photometric observations are presented in Figure 2. In this particular case we use the time of the non-detection for the explosion time, which is sufficiently close to our preferred time that the qualitative features are unchanged. In the top panel we compare the inferred bolometric lightcurve (filled circles) to the model fit (solid curve). We also plot the contributions from direct heating L_{56} (dashed curve) and the diffusive tail L_{tail} (dotted curve). The direct heating component is larger at late times and the diffusive tail is stronger at early times when the ^{56}Ni is less abundant. Nevertheless, L_{tail} is never more than a factor of two greater than L_{56} . This means that at least very roughly, the observed bolometric luminosity can be used to infer the distribution of ^{56}Ni , and that ^{56}Ni must be present, at least in some amount, at the depths that are probed by the earliest emission.

The middle panel of Figure 2 shows the inferred color temperature T_c , and the bottom panel shows the mass of ^{56}Ni above the diffusion wave depth, given by

$$M_{56}(t) = L_{56}(t)/\epsilon(t). \quad (14)$$

This is roughly independent of the explosion time because it is just set by the bolometric luminosity at any given time. In

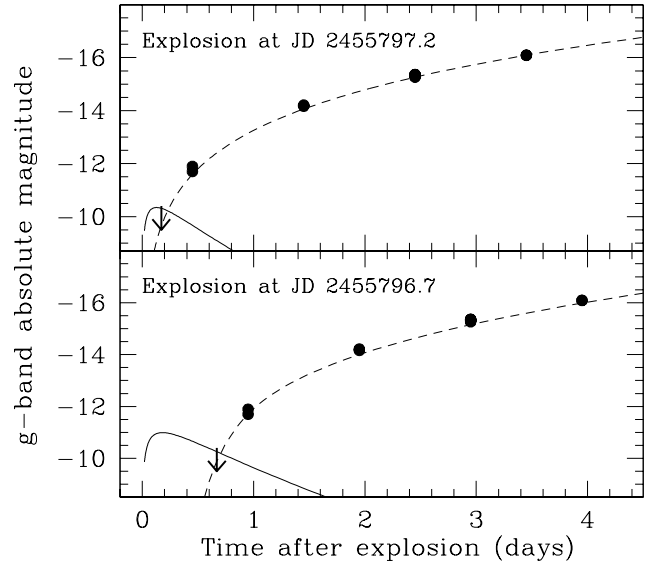


FIG. 3.— Comparison of the early g -band data (Nugent et al. 2011) and a non-detection upper limit (Bloom et al. 2012) to theoretical lightcurves from radioactive heating (dashed curves) and shock-heated cooling (solid curves) calculated according to Piro et al. (2010). This does not include the suppression of the shock-heated cooling (or “drop out”) that occurs when the diffusion wave moves into ideal gas dominated material (Rabinak et al. 2012). The top panel is roughly the explosion time inferred from a t^2 extrapolation. The bottom panel assumes that the explosion occurred 0.5 days earlier, for which the radius constraint is a factor of 1.9 larger.

contrast, T_c changes with explosion time because an explosion further in the past implies more expansion at any given time and thus a smaller T_c . This means that an additional constraint on the explosion time could be made via a temperature measurement, although this requires detailed spectral modeling that is outside the scope of this work (see the discussion of t_{min} in Piro & Nakar 2012).

3.2. Radius Constraints and Shallowest ^{56}Ni for SN 2011fe

Using the data from Nugent et al. (2011) and a non-detection ≈ 7 hrs earlier, Bloom et al. (2012) argued that the progenitor of SN 2011fe had a radius $\lesssim 0.02R_{\odot}$ by using models of shock-heated cooling (Piro et al. 2010; Rabinak et al. 2012). But this assumed that the time of explosion could be accurately determined from extrapolating t^2 back in time. As emphasized in Piro & Nakar (2012), this is not generally a robust method for finding the explosion time (see also §4), so it is worth revisiting the radius constraint for a range of explosion times.

In Figure 3 we plot the early data and non-detection upper limit for SN 2011fe for two different explosion times. The theoretical curves include radioactive heating (dashed curves) and shock-heated cooling (solid curves). The first thing to note is that ^{56}Ni cannot always be present at the earliest times and still produce the observed lightcurves. In the bottom panel we had to cut off the ^{56}Ni for times earlier than 0.9 days after explosion in order to not overpredict the g -band upper limit reported in Bloom et al. (2012). (In the top panel no ^{56}Ni cut-off is needed.) This implies that for earlier explosion times there is a sharp cut-off in the ^{56}Ni distribution near the depth that generates the luminosity of the first detected light. This is not unexpected since ^{56}Ni probably does not extend to the very surface and the earliest emission will be due to the diffusive tail. In §3.5 we further discuss what depth in the

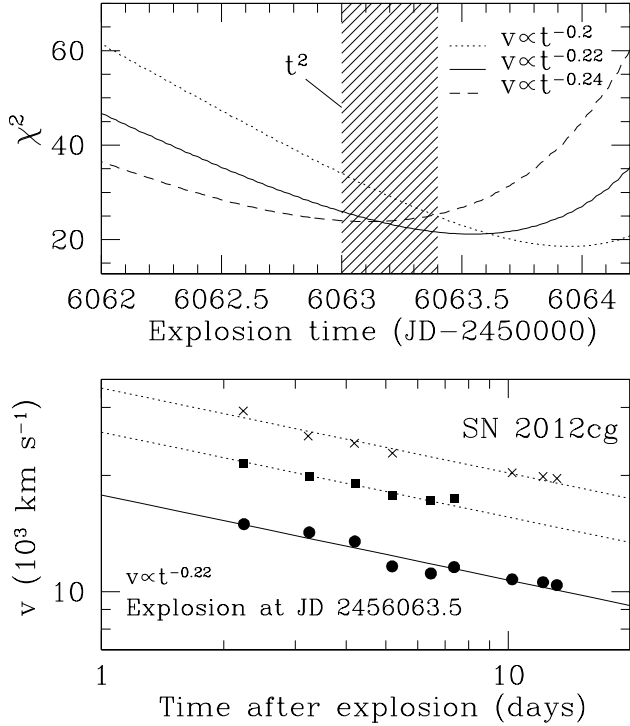


FIG. 4.— The same as Figure 1, but for SN 2012cg. The shaded region shows the inferred explosion time from Silverman et al. (2012) using t^2 .

WD is implied by this time.

The other thing to note from Figure 3 is that when the explosion time is further in the past, upper limits on the emission from shock-heated cooling (solid curves) are not as stringent. Using the models from Piro et al. (2010) we find that when the explosion is merely 0.5 days further in the past (the bottom panel) the radius can be a factor of 1.9 greater than in the top panel.

Another potentially important effect that is not included in Figure 3 is the “drop out” in the shock-heated cooling emission that is expected once the diffusion wave exposes the depth where the shock is matter rather than radiation dominated. This is expected to occur \sim hours after explosion for a typical WD radius (Rabinak et al. 2012). Although we do not consider explosion times earlier than the non-detection of Nugent et al. (2011) in Figure 3, it is possible that the explosion occurred before (\sim 0.5 day) this time, and the non-detection is simply during the dark phase between the drop out and the latter ^{56}Ni heating. Bloom et al. (2012) find that the drop out limits the radius constraint posed by their upper limit. If the explosion is one day before the date estimated by Nugent et al. (2011), then the uncertainty in the limit on the radius of the progenitor of SN 2010fe is only $\sim 0.1R_{\odot}$.

3.3. SN 2012cg

The velocities and photometry for SN 2012cg are summarized in Silverman et al. (2012). Further photometry is presented by Munari et al. (2012), including data around the peak identified to occur at roughly JD 2456083.0. The velocity fitting results are shown Figure 4 (again taking $\Delta v = 500 \text{ km s}^{-1}$). The best fit explosion time is JD 2456063.5, but the strength of the fit is not as strong as for SN 2011fe. In comparison, using t^2 Silverman et al. (2012) find JD 2456063.2 ± 0.2 (the shaded region in the top panel of

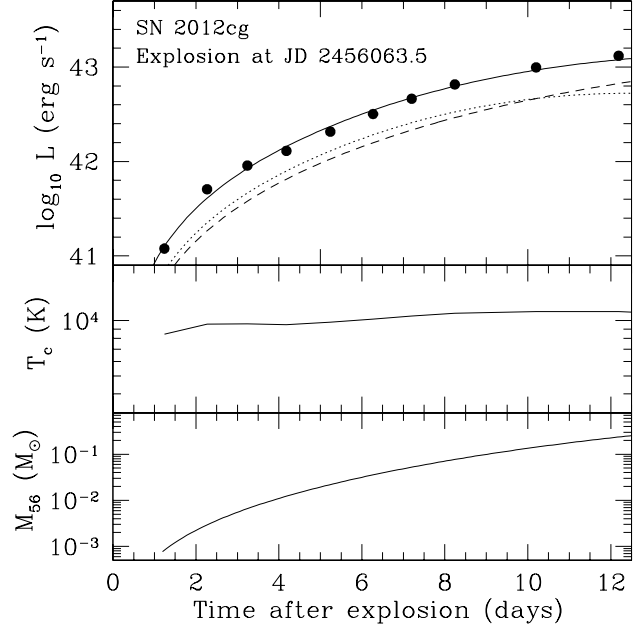


FIG. 5.— The same as Figure 2, but for SN 2012cg.

Figure 4), which is consistent with our fits. The lightcurve modeling from the observed B , V , and R measurements use a distance modulus of 30.9. The summary of our results from the photometric data are presented in Figure 5.

3.4. SN 2009ig

The velocities and photometry for SN 2009ig are presented in Foley et al. (2012). The time of B -band peak is at JD 2455080.54, and the distance modulus is 32.6. The evolution of the Si II $\lambda 6355$ absorption feature is a little more complicated in this case and deserves some discussion. At early times (earlier than 12 days before B -band peak), Si II appears to only have a high velocity component, and a low velocity component grows to be more prominent later. We take the low velocity component as indicative of the photosphere, but use both the high and low velocity components when fitting the $v \propto t^{-0.22}$ power law. Data taken when the features overlap could potentially bias the fit due to blending, but we did not find that it has an adverse impact on our fits.

In Figure 6 we summarize the velocity fitting. Only high and low velocity Si II are used in this case. High-velocity Ca II H&K absorption features may be blended with Si II $\lambda 4130$, and are not presented by Foley et al. (2012). The best fit time of explosion is at JD 2455061.8. In comparison, using a t^2 rise Foley et al. (2012) infer an explosion time JD 2455063.4 ± 0.07 . Although SN 2009ig has the least constraining fits of any of the SNe, this later explosion time seems difficult to reconcile with the velocity evolution unless $v(t)$ is a much shallower power law with time than that expected from theory. In Figure 7 we plot the best fit lightcurve properties as was done for the other SNe.

3.5. Comparing and Contrasting Events

In Figure 8 we plot the distributions of ^{56}Ni inferred for the three SNe Ia modeled above. In each case multiple values for the explosion time are considered to demonstrate how inferences on X_{56} change with this parameter. The solid lines in each panel indicate the preferred explosion time. For SN

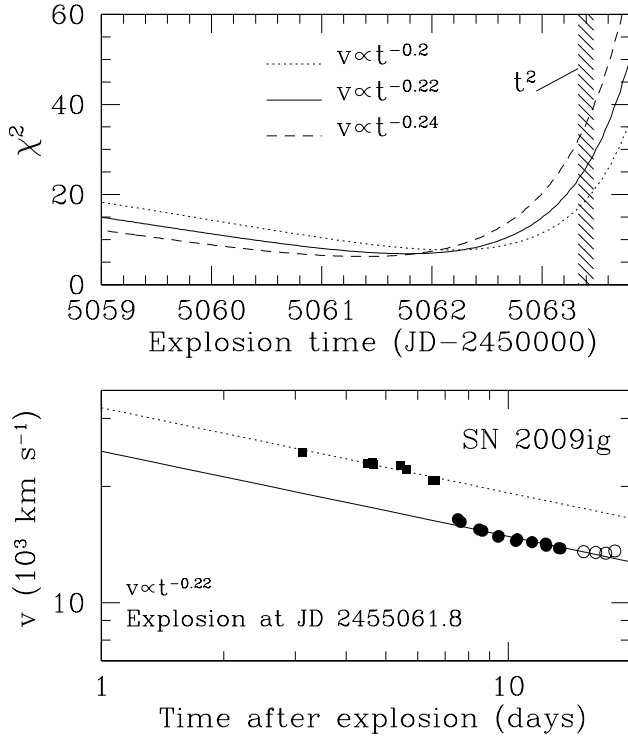


FIG. 6.— The same as Figure 1, but for SN 2009ig. Open circles indicate data that was not used for the fit because they are too close to peak. Although an explosion time of JD 2455061.8 is favored, the constraints are not as strong as for the other SNe.

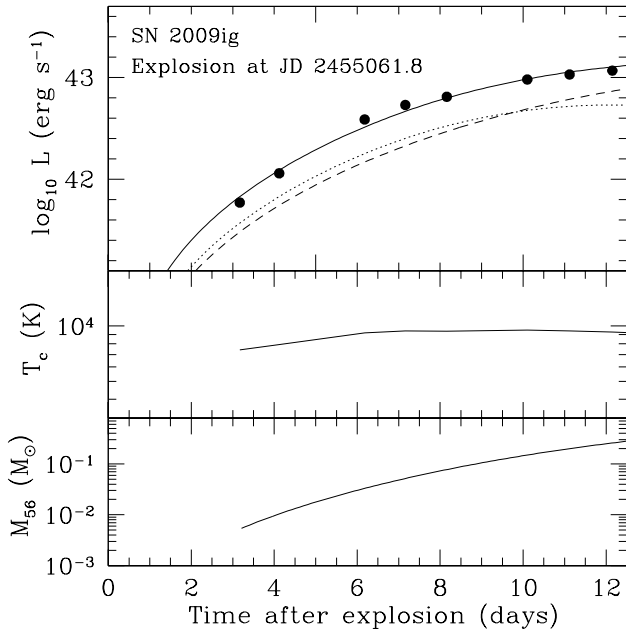


FIG. 7.— The same as Figure 2, but for SN 2009ig.

2011fe (top panel), thick lines show the distribution covered by the photometric observations of Vinkó et al. (2012) and thin lines show the distribution inferred by the earlier observations by Nugent et al. (2011). This shows that since $\Delta M_{\text{diff}} \propto t^{1.76}$, having observations just a day or two earlier can probe much shallower regions of the ejecta. For the preferred explosion time, $X_{56} \approx 3 \times 10^{-2}$ at a depth of

$\Delta M_{\text{diff}} \approx 10^{-2} M_{\odot}$. These results are roughly consistent with models presented by Piro (2012), which assumed a similar explosion time but did not include the diffusive tail. As discussed in §3.2, the upper limit on the luminosity at early times implies that there must be a cut-off in the ^{56}Ni distribution for some explosion times. These shallowest ^{56}Ni depths are indicated by filled circles in the top panel of Figure 8 (although not mentioned in §3.2, for the -0.5 days curve, ^{56}Ni cannot be shallower than 1.7 days after the explosion).

The ^{56}Ni distributions in SN 2012cg and SN 2009ig are fairly similar to SN 2011fe over similar depths. The main difference is that SN 2012cg shows somewhat more ^{56}Ni around a range of $\Delta M_{\text{diff}} \approx 10^{-2} - 10^{-1} M_{\odot}$. Does this imply that SN 2012cg has more shallow burning products? Analysis of the spectra indicate that SN 2011fe has considerably more unburned carbon at shallow depths than SN 2012cg (Parrent et al. 2012), which is at least consistent with this hypothesis.

SN 2009ig also has a number of differences that are worth discussing. The Si II velocities at ≈ 10 days past explosion are considerably higher in this event than either SN 2011fe or SN 2012cg. If this indicates a difference in the actual explosion energy, then using $v_{\text{ph}} \propto E^{0.39}$ (Piro & Nakar 2012) argues that SN 2009ig was a factor of ≈ 2 more energetic than the other two events. Such an explanation seems difficult to reconcile with the peak luminosity of SN 2009ig, which is fairly standard for SNe Ia. Another attractive possibility is that the large velocities are due to an asymmetric explosion that is directed more toward the observer (Maeda et al. 2010a). For such larger velocities, there is more expansion and a generally cooler SN, as can be seen by the T_c presented in the middle panel of Figure 7. Foley et al. (2012) note that SN 2009ig is considerably redder in the UV at early times in comparison to other SNe Ia and typical templates. Is this just due to the larger velocities? Another possibility is that these colors are due iron-peak elements near the surface, which again would be consistent with an explosion directed toward the observer. The mass fraction of ^{56}Ni for SN 2009ig is fairly similar to the other SNe at a depth of $\approx 0.1 M_{\odot}$, and data is not available early enough to probe shallower regions.

Although the many differences found for SN 2009ig are tantalizing, we emphasize that these conclusions all hinge on our assumption that roughly $v \propto t^{-0.22}$. If for some reason the velocity profile of SN 2009ig is different than the other two SNe, then these conclusions must be revised. On the other hand, if the velocity profile is significantly different in this case, that might be interesting in and of itself.

3.6. Progenitor Models

For all three SNe we study, ^{56}Ni must be present at least $\approx 0.1 M_{\odot}$ from the WD surface, and as shallow as $\approx 10^{-2} M_{\odot}$ from the surface for SN 2011fe and SN 2012cg (see Figure 8). It is therefore worth discussing the implications for progenitor models and the character of the explosive burning.

As a comparison, Hachinger et al. (2012) performed detailed UV/optical spectral modeling of SN 2010jn. From this analysis they also infer iron-group elements near the surface. DDT models can produce ^{56}Ni near the WD surface (e.g., Iwamoto et al. 1999), but to get radioactive material as shallow as $\approx 10^{-2} M_{\odot}$ may require a strongly mixed, off-center deflagration (Maeda et al. 2010b). In DDT models with many ignition points that have fairly stratified ashes, radioactive elements are not present near the surface. A gravitationally con-

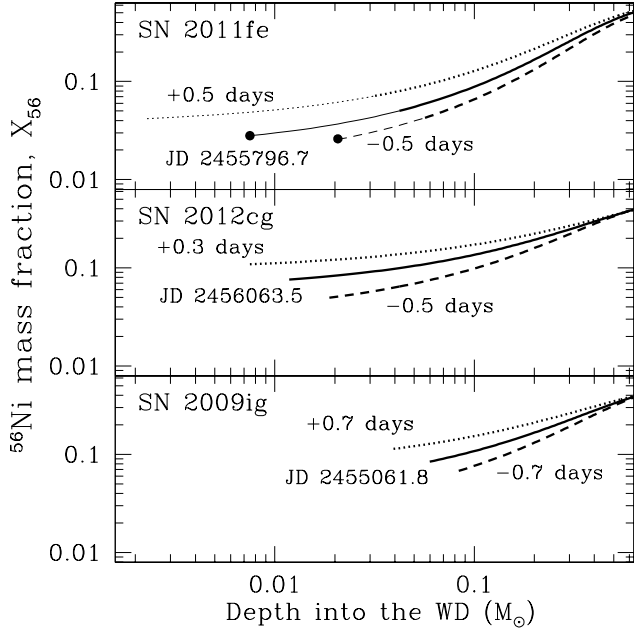


FIG. 8.— Inferred distribution of ^{56}Ni as a function of depth in the WD. In each case we compare multiple explosion times, with the solid lines indicating the value preferred by fitting $v \propto t^{-0.22}$. The depth into the star is assumed to scale as $\Delta M_{\text{diff}} \propto t^{1.76}$ with a normalization of $\Delta M_{\text{diff}} = 1.4M_{\odot}$ at lightcurve peak. For SN 2011fe (top panel), the thick curves correspond to the constraints from the observations by Vinkó et al. (2012), and the thin curves correspond to the observations by Nugent et al. (2011). The filled circles indicate the shallowest allowed deposits of ^{56}Ni so as not to overshoot the upper limit presented by Bloom et al. (2012).

finned detonation also produces iron-peak elements near the surface when a bubble rises and breaks (Meakin et al. 2009).

Another interesting scenario that may produce shallow radioactive heating is the explosive ignition of a helium shell in a double-detonation. The depth and amount of ^{56}Ni we infer is not dissimilar to the helium shell masses needed for detonation and the total amount of radioactive material found for such events (Shen & Bildsten 2009; Fink et al. 2010). The main problem with such models is that if iron-peak elements are too abundant, they tend to produce colors that are too red and spectra that are inconsistent with normal SNe Ia (Kromer et al. 2010; Sim et al. 2012). But if the helium burns in a lateral detonation which does not process the fuel as completely to iron-peak elements (Townsend et al. 2012), this may overcome some of the difficulties double-detonation models have in reproducing observed SNe Ia.

4. IS A t^2 RISE SPECIAL?

A common practice with recent SN Ia observations is to determine the time of explosion by fitting the rising luminosity (often in a single band) with a t^2 curve (Nugent et al. 2011; Milne & Brown 2012; Foley et al. 2012; Silverman et al. 2012). Studies of composite lightcurves formed from stacking many SNe, which allow the power-law index to vary, find power-law indices of 1.8 ± 0.2 (Conley et al. 2006), $1.8^{+0.23}_{-0.18}$ (Hayden et al. 2010), and $2.20^{+0.27}_{-0.19}$ (Ganeshalingam et al. 2011). This then begs the question, is t^2 (or any other power-law) fundamental, and if not, what is the origin of these results?

Our discussion in §2 shows that a priori a power-law luminosity rise is not generally expected. The luminosity is driven

by a combination of two factors: (i) the diffusion wave propagation, $\Delta M_{\text{diff}}(t)$, and (ii) the distribution of ^{56}Ni fraction, X_{56} . The exposed mass does indeed evolve as a power law, with (Piro 2012)

$$\Delta M_{\text{diff}}(t) \propto t^{2(1+1/n)/(1+1/n+\beta)}, \quad (15)$$

where n is the polytropic index and β is the power-law index of the velocity gradient. For $n = 3$ and $\beta = 0.186$ (Sakurai 1960), this results in $\Delta M_{\text{diff}} \propto t^{1.76}$ (as in eq. [1]). In contrast, the ^{56}Ni distribution is not well constrained by theory and may, in principle, vary in many ways. A power-law rise of the bolometric luminosity is expected only if the ^{56}Ni fraction evolves as a power-law as well, namely $X_{56} \propto t^{\alpha}$. In this case the bolometric luminosity evolves as $L \propto t^{1.76+\alpha}$ and since the photospheric radius is roughly $\propto t^{0.78}$ (Piro & Nakar 2012), the observed temperature evolves roughly as $T_c \propto t^{(0.2+\alpha)/4}$. This result was obtained by Piro (2012) when the diffusive tail was not included, and we find that it still holds with the more detailed analysis presented in §2. Since we do not expect $X_{56} \propto t^{0.24}$, our conclusion is that a t^2 rise (bolometric or in a single band) is probably not a generic property of SNe Ia. We also do not expect the rise to follow exactly any other power law. Moreover, since most explosion models predict a sharp decrease of X_{56} in the outermost layers of the ejecta, the lightcurve is expected to rise exponentially (due to diffusive tail contribution) at very early times. How early this exponential phase take place depends on the depth of the shallowest ^{56}Ni deposit.

What is then the explanation of the fact that analysis of large SNe samples are found to be consistent with a power-law rise with indices in the range $\approx 1.8 - 2.2$? It is probably a combination of two things. First, the unknown explosion time enables a reasonable fit even if the lightcurve is not exactly a power law. Second, in the depth range explored by most of these SNe rising phases, the X_{56} is not varying by a large amount. This is because the first observation of most SNe Ia take place only a few days to a week after the explosion, so that the ^{56}Ni is distributed roughly uniformly or slowly increasing with depth.

In Figure 9, we plot the bolometric lightcurves and fits for the three SNe we have been studying on a logarithmic scale to emphasize power-law dependencies. This shows that the lightcurves are not rising exactly as power laws, but that power law fits can provide a reasonable description of the data (although for SNe 2011fe the rise is found to be slightly faster than t^2). This is because in all three of these SNe the X_{56} is rising rather gradually over the depth range probed by the observations.

There have been some attempts to explain why there should be a t^2 rise, but none of these provide arguments that are expected to hold in detail. The most simplified explanation is a fixed color temperature with a radius that increases linearly with time (Riess et al. 1999). This model does not explain why the temperature should be constant, and more importantly, in real SNe the color temperature does typically vary with time. A more fundamental explanation for a t^2 rise is given in the Supplementary Information of Nugent et al. (2011), which considers radioactive heating with thermal diffusion (also see Arnett 1982). This model makes two explicit approximations: (i) it ignores the velocity gradient, obtaining $\Delta M_{\text{diff}} \propto t^2$ (basically setting $\beta = 0$ in eq. [15]), and (ii) it assumes that X_{56} is constant. Together these factors result in

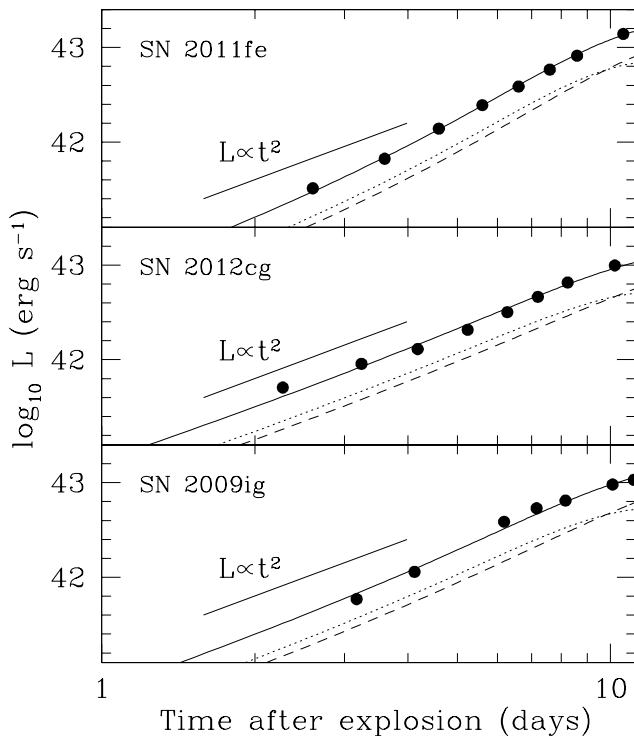


FIG. 9.— The bolometric lightcurves for each of the three SNe (from the top panels of Figures 2, 5, and 7), but in this case plotted with logarithmic axes to emphasize power-law behavior.

a t^2 rise, but only for assumptions that are not realistic.

To conclude, we expect the early rise to depend on the particular physical conditions in any given event and thus to possibly vary from one SN to another. It will be important to test this hypothesis in the future by building bolometric lightcurves from observations to infer just how much diversity there really is. Detailed numerical calculations of the rise will also be useful for understanding how much the early luminosity can change depending on composition and radiative transfer effects. Whatever the results are, extrapolating a lightcurve back in time with t^2 is not a reliable method for inferring the explosion time.

5. CONCLUSIONS AND DISCUSSION

Using early observations of three SNe Ia, and assuming that the absorption feature velocities evolve as $v \propto t^{-0.22}$, we constrained the explosion times and shallow distributions of ^{56}Ni . We then used these findings to revisit the radius constraints on the progenitor of SN 2011fe (in §3.2), and discuss the t^2 rise that is reported for many SNe Ia (in §4). Our general conclusion is that SN 2011fe and SN 2012cg are very similar in most

respects, including the rise time, ^{56}Ni distribution, and energetics. The main difference is that SN 2012cg has a slightly larger amount of shallow ^{56}Ni .

SN 2009ig is somewhat different than the other two SNe. Although its ^{56}Ni distribution over the same depths probed in SN 2011fe and SN 2012cg are fairly similar, it has higher velocities at any given time and its best fit time of explosion has the largest discrepancy with previous estimates (≈ 1.6 days earlier). This is curious because the peak luminosity of SN 2009ig is fairly normal in comparison to the other SNe, and thus the amount of ^{56}Ni and the energetics should be similar. One possible solution is if SN 2009ig is asymmetric with higher velocities directed toward the observer (Maeda et al. 2010a). Unfortunately our results on SN 2009ig are somewhat tentative because it has the least constrained time of explosion. This is because the low velocity Si II is only seen relatively late, and thus has a rather flat evolution with time. Hopefully our work inspires more detailed modeling of SN 2009ig in the future to test our conclusions.

These comparisons show how important it is to have the earliest observations possible. Out the events we consider, SN 2011fe is the best constrained because it shows the largest velocity gradients. Just a few velocity measurements very early in the lightcurve can be more helpful in determining the explosion time than having many measurements at later times. Furthermore, since $\Delta M_{\text{diff}} \propto t^{1.76}$, having observations only a day or two earlier probe much shallower depths in the ejecta. Although not discussed much here, having one or two early spectra that can be used for modeling the surface temperature can also provide tight constraints on the explosion time (Piro & Nakar 2012).

With just these three events, we are already beginning to see correlations between the various features that determine the early lightcurve rise. In the future, studies should look for connections between the early rise and a larger range of properties, such as the late nebular features or the characteristics of the host galaxies. It will also be useful to compare spectral modeling methods for measuring surface abundances (like in Hachinger et al. 2012) with the techniques we present here. If used together, they may be more constraining on the nature of the progenitors and the details of the explosive burning. Finally, it would be worth exploring the early lightcurves of non-standard SNe Ia, like SN 2002cx (Li et al. 2003). Such studies will be important for fully utilizing the observations available in this new era of early detections of exploding WDs.

We thank Ryan Foley, Mohan Ganeshalingam, and Jeffrey Silverman for assistance with assessing data and discussing observations. We also thank Federica Bianco, Ryan Chornock, Luc Dessart, Stephan Hachinger, Keiichi Maeda, Peter Nugent, and Re'em Sari for helpful discussions or comments on previous drafts. ALP was supported through NSF grants AST-1212170, PHY-1151197, and PHY-1068881, NASA ATP grant NNX11AC37G, and by the Sherman Fairchild Foundation. EN was partially supported by an ERC starting grant (GRB-SN 279369).

REFERENCES

- Arnett, W. D. 1982, *ApJ*, 253, 785
 Bloom, J. S., Kasen, D., Shen, K. J., et al. 2012, *ApJ*, 744, L17
 Conley, A., Howell, D. A., Howes, A., et al. 2006, *AJ*, 132, 1707
 Fink, M., Röpke, F. K., Hillebrandt, W., et al. 2010, *A&A*, 514, A53
 Foley, R. J., Challis, P. J., Filippenko, A. V., et al. 2012, *ApJ*, 744, 38
 Ganeshalingam, M., Li, W., & Filippenko, A. V. 2011, *MNRAS*, 416, 2607
 Hachinger, S., Mazzali, P. A., Sullivan, M., et al. 2012, arXiv:1208.1267
 Hayden, B. T., Garnavich, P. M., Kessler, R., et al. 2010, *ApJ*, 712, 350
 Hillebrandt, W., & Niemeyer, J. C. 2000, *ARA&A*, 38, 191
 Hoyle, F., & Fowler, W. A. 1960, *ApJ*, 132, 565
 Iben, I., Jr., & Tutukov, A. V. 1984, *ApJS*, 54, 335
 Iwamoto, K., Brachwitz, F., Nomoto, K., et al. 1999, *ApJS*, 125, 439

- Khokhlov, A. M. 1991, *A&A*, 245, 114
- Kromer, M., Sim, S. A., Fink, M., et al. 2010, *ApJ*, 719, 1067
- Li, W., Filippenko, A. V., Chornock, R., et al. 2003, *PASP*, 115, 453
- Livne, E., & Arnett, D. 1995, *ApJ*, 452, 62
- Maeda, K., Benetti, S., Stritzinger, M., et al. 2010a, *Nature*, 466, 82
- Maeda, K., Röpke, F. K., Fink, M., et al. 2010b, *ApJ*, 712, 624
- Meakin, C. A., Seitenzahl, I., Townsley, D., et al. 2009, *ApJ*, 693, 1188
- Milne, P. A., & Brown, P. J. 2012, arXiv:1201.1279
- Munari, U., Henden, A., Belligoli, R., et al. 2012, arXiv:1209.4692
- Nakar, E., & Sari, R. 2010, *ApJ*, 725, 904
- Nakar, E., & Sari, R. 2012, *ApJ*, 747, 88
- Nomoto, K., Sugimoto, D., & Neo, S. 1976, *Ap&SS*, 39, L37
- Nomoto, K., Thielemann, F.-K., & Yokoi, K. 1984, *ApJ*, 286, 644
- Nugent, P. E., Sullivan, M., Cenko, S. B., et al. 2011, *Nature*, 480, 344
- Parrent, J. T., Howell, D. A., Friesen, B., et al. 2012, *ApJ*, 752, L26
- Patat, F., Cordiner, M. A., Cox, N. L. J., et al. 2011, arXiv:1112.0247
- Perlmutter, S., Aldering, G., Goldhaber, G., et al. 1999, *ApJ*, 517, 565
- Pinto, P. A., & Eastman, R. G. 2000, *ApJ*, 530, 757
- Piro, A. L., Chang, P., & Weinberg, N. N. 2010, *ApJ*, 708, 598
- Piro, A. L. 2011, *ApJ*, 738, L5
- Piro, A. L. 2012, *ApJ*, 759, 83
- Piro, A. L., & Nakar, E. 2012, arXiv:1210.3032
- Rabinak, I., Livne, E., & Waxman, E. 2012, *ApJ*, 757, 35
- Richmond, M. W., & Smith, H. A. 2012, *Journal of the American Association of Variable Star Observers (JAAVSO)*, 216
- Riess, A. G., Filippenko, A. V., Challis, P., et al. 1998, *AJ*, 116, 1009
- Riess, A. G., Filippenko, A. V., Li, W., et al. 1999, *AJ*, 118, 2675
- Sakurai, A. 1960, *Commun. Pure Appl. Math.*, 13, 353
- Shappee, B. J., & Stanek, K. Z. 2011, *ApJ*, 733, 124
- Shen, K. J., & Bildsten, L. 2009, *ApJ*, 699, 1365
- Silverman, J. M., Ganeshalingam, M., Cenko, S. B., et al. 2012, *ApJ*, 756, L7
- Sim, S. A., Fink, M., Kromer, M., et al. 2012, *MNRAS*, 420, 3003
- Tanaka, M., Mazzali, P. A., Benetti, S., et al. 2008, *ApJ*, 677, 448
- Townsley, D. M., Moore, K., & Bildsten, L. 2012, *ApJ*, 755, 4
- Vinkó, J., Sárneczky, K., Takáts, K., et al. 2012, *A&A*, 546, A12
- Webbink, R. F. 1984, *ApJ*, 277, 355
- Whelan, J., & Iben, I., Jr. 1973, *ApJ*, 186, 1007
- Woosley, S. E., & Weaver, T. A. 1994a, *ApJ*, 423, 371
- Woosley, S. E., & Weaver, T. A. 1994b, in *Les Houches Session LIV, Supernovae*, ed. S. Bludman, R. Mochovitch, & J. Zinn-Justin (Amsterdam: North Holland), 63